Conduction mechanism of an infrared emitting diode: impedance spectroscopy and current–voltage analysis

© Adem Dönmez, Habibe Bayhan¶

Muğla University, Faculty of Arts and Sciences, Department of Physics,
48000 Muğla, Turkey

The bias dependent complex impedance spectra of a conventional GaAs based infrared emitting diode have been studied in the temperature range 150–300 K. It is found that for bias voltages lower than 0.7 V, the device behaves like a pure capacitor. However for $V_{dc} \geq 0.7$ V, an equivalent circuit model composed of a parallel resistor (R_p) and capacitor (C_p) network connected with a series resistance (R_s) can be used to describe the individual impedance contributions from interfacial and bulk regions of the diode. Fitting of experimental data to the proposed ac model reveal that the value of parallel device capacitance C_p increases with temperature whereas the parallel resistance R_p component decreases. The tendency of parallel resistance and parallel capacitance as a function of temperature is expected that thermally activated current transport mechanism dominates in the forward bias, which coincides with the analysing results of the dark forward current–voltage (I–V) characteristics. The temperature dependent I–V variations suggest that recombination in the depletion region has a paramount role.

1. Introduction

Semiconductor based light sources in the infrared (IR) spectral region are of considerable interest for their potential use in the electrical communication technology as a wireless optical interconnection and switch component [1–3] and in the infrared imaging applications [4]. Although a number of studies were conducted on the direct current (dc) and alternating current (ac) electrical properties of IR emitting diode structures under dark and illuminated conditions, limitations on the electronic transport process associated with junction interface is still the largest issue for the efficient and reliable device operation. Modelling the frequency response of a p–n junction device with an electrical analogue circuit can yield useful information about the dynamic electronic nature of the junction interface and the mechanisms underlying for ac transport properties.

Impedance spectroscopy (IS) is a powerful customary experimental tool which can be invoked to probe the ac behaviour of dielectric layers, organic and inorganic materials and solid state devices [5–9]. Impedance measurements of light emitting devices is an increasingly popular technique, however, the majority of these measurements to date have been carried out at different bias values on organic based devices [10–12]. To our knowledge particularly there is very limited publication on the impedance spectroscopic and current transport analysis of IR emitting semiconductor devices. In this study, a detailed study of a conventional GaAs based infrared emitting diode by complex impedance spectroscopy in the frequency range from 100 Hz to 10 MHz as a function of temperature and voltage is presented. The static electrical transport properties of the device are also investigated in the dark by temperature dependent current–voltage measurements.

2. Experimental

The dark ac impedances of a conventional GaAs based infrared emitting diode were measured with the dc bias voltages (V_{dc}) from 0 to 1.0 V using a Hewlett Packard HP 4192A impedance analyzer in the frequency (f) range from 10 Hz to 10 MHz. Since CQY37N is a non-linear device, the amplitude of the applied signal should be less than thermal voltage ($V_T \approx 26$ mV at 22°C). The ac signal of amplitude 10 mV is selected to ensure that the response of the system is linear piecewise to good approximation. The shield cables were used for the connections to reduce noise from the environment. The device was mounted in the sampler holder of the helium cryostat (Oxford) and all measurements are performed in vacuum. The temperature T of the sample holder was varied from 150 to 300 K in steps of 10 K using ITC 502 temperature controller. A Keithley 236 source–measure unit is also used for temperature dependent (100–300 K) current vs. voltage measurements in the dark.

3. Results and discussions

The impedance spectroscopy data $Z(\omega)$ taken at different temperatures ($150 < T < 300$ K) and at dc bias voltages below than 0.7 V for the infrared emitting (IR) diode has shown a linear variation (not shown here) almost perpendicular to the real impedance axis. Their $\lg|Z| = \sqrt{(\mathrm{Re}\, Z)^2 + (\mathrm{Im}\, Z)^2}$ vs. $\lg f$ (frequency) variations (not shown here), also yield a straight line over the whole frequency range under consideration. All these indicate that the typical device behaves like a pure capacitor for $V_{dc} < 0.7$ V in the whole temperature range considered. Since the impedance of a pure capacitor with capacitance C, is given as

$$Z = \mathrm{Re}\, Z + j\mathrm{Im}\, Z = -j\,\frac{1}{\omega C} = -j\left(\frac{1}{2\pi f C}\right) \qquad (1)$$

where $\omega = 2\pi f$ is the angular frequency of the ac signal, $\mathrm{Re}\, Z$ and $\mathrm{Im}\, Z$ are the real and the imaginary parts, respectively with $j = \sqrt{-1}$. Based on Eq. (1) and high frequency (1 MHz) room temperature impedance data mea-

¶ E-mail: hbayhan@mu.edu.tr

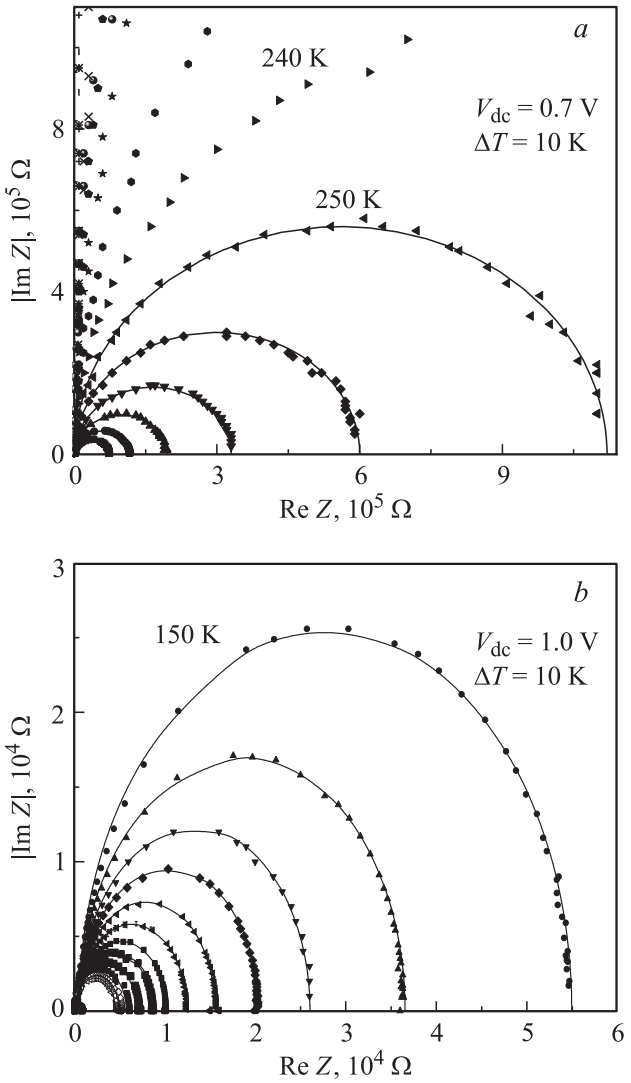

Figure 1. Temperature dependent $|\mathrm{Im}\, Z|$ vs. $\mathrm{Re}\, Z$ plots at (*a*) 0.7 V and (*b*) 1.0 V. The solid lines represent the fit to the equivalent circuit model given in Fig. 2.

sured at zero dc voltage, a capacitance value of about 32 pF is inferred for the IR emitting diode. This value is almost the same with the value estimated by admittance spectroscopy technique and approximately in well agreement with the value 50 pF, reported in the data sheet [1].

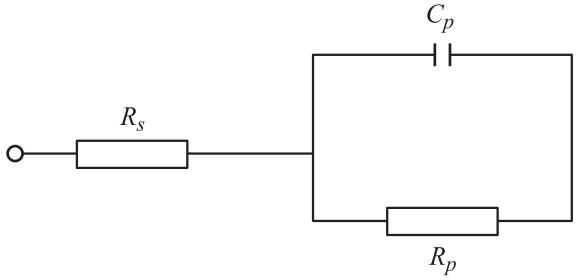

Figure 2. Proposed equivalent circuit model.

The complex impedance $|\mathrm{Im}\, Z|$ versus $\mathrm{Re}\, Z$ plots of the IR emitting diode at selected dc voltages $V_{dc} = 0.7$ and 1.0 V are shown in Figs. 1, *a* and *b*, respectively. At 0.7 V, a complete semicircular behaviour is commenced as the temperature is increased approximately above than 240 K. This could be related to decrease in the resistance of the space charge region as a result of increase in the charge carrier injection. As it is seen typically in Fig. 1, (*b*), if $V_{dc} > 0.7$ V, then all temperature dependent (150–300 K) complex impedance characteristics can be characterised by a semicircular shape apparently composed by a single time constant. This semicircular nature of the impedance characteristics indicates that the ac equivalent circuit of the device consists of a parallel connection of an ohmic resistor R and a capacitor C. In addition, the minimum $\mathrm{Re}\, Z$ values at the highest frequency ($\sim 2 \cdot 10^6$ Hz) are found be different from zero which represent that there should be a series resistance to the predicted parallel RC network. Thus the complete equivalent circuit for the device can be designed as a parallel resistor R_p and capacitor C_p network connected with a series resistance R_s as illustrated in Fig. 2. It can be observed from Figs. 1, *a* and *b*, that the proposed equivalent circuit model which is given by a solid line shows a good agreement with the experimental data.

It is generally assumed that the R_pC_p network simulates the response from the interface of the junction region and series resistance R_s represents all ohmic contributions due to the device bulk and the ohmic contacts. The real and the imaginary components of this simple equivalent circuit (see Fig. 2) are as follows;

$$\mathrm{Re}\, Z = R_s + \frac{R_p}{1 + \omega^2 R_p^2 C_p^2}$$

$$\mathrm{Im}\, Z = \frac{\omega R_p^2 C_p}{1 + \omega^2 R_p^2 C_p^2}. \qquad (2)$$

The equivalent capacitive effect $C_p = C_T + C_d$ of this R_pC_p network could possibly be assumed to be raised due to the gradient of charge density inside the device, C_p (diffusion capacitance) and the space charge capacitance, C_T (transition capacitance) [13]. The equivalent parallel resistance, R_p; $R_d \parallel R_T$ could then be caused by the bulk resistance of the space charge region, R_d and the resistance due to recombination of free carriers in the space charge region, R_T [13]. The typical value of the equivalent capacitance $C_T + C_d$ at a given temperature is first roughly estimated by using the value of frequency f at maximum of $\mathrm{Im}\, Z$ [14] i. e.,

$$(\mathrm{Im}\, Z)_{\max} = \frac{1}{2\pi f (C_d + C_T)}$$

and then optimized by theoretical fitting to the proposed ac equivalent circuit. The rough values of R_s and $R_s + R_p$ are estimated from the low and high frequency intercepts of the semicircular variations on the $\mathrm{Re}\, Z$ axis of complex impedance plots, respectively and then further improved with theoretical fitting.

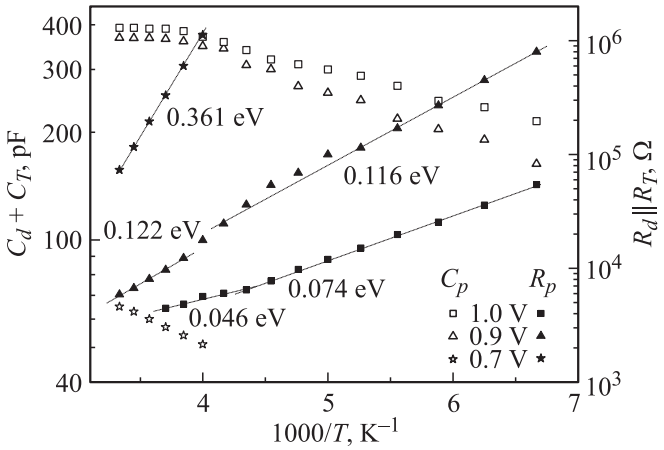

Figure 3. The variation of equivalent capacitance $C_T + C_d$, and resistance $R_d \parallel R_T$, as a function temperature for different dc bias voltages: 0.7, 0.9 and 1.0 V.

To understand the temperature and the voltage dependent natures of the equivalent circuit parameters, both $R_d \parallel R_T$ and $C_T + C_d$ values estimated at 0.7, 0.9 and 1.0 dc bias voltages are plotted against temperature as shown in Fig. 3. As it is seen from this figure that approximately above 270 K, the typical $C_T + C_d$ variation is relatively insensitive to the temperature and below 270 K the equivalent capacitance decreases as the temperature decreases at 0.9 and 1.0 V dc bias voltages. On the other hand, C_p is found to increase with applied temperature for $T > 250$ K at 0.7 V. Since space charge capacitance is caused by ionized charges stored in the depletion region, the value of C_T is expected to be almost unchanged with temperature as observed at relatively high temperatures for 0.9 and 1.0 V in Fig. 3 [13,14]. The strong dependence of C_p on the temperature (for $T < 270$ K at 0.9 and 1.0 V and for $T > 250$ K at 0.7 V) can be ascribed to the contribution of diffusion capacitance [14,15] and most probably the presence of trapping states responding to the applied ac signal [16]. It is possible that such an almost linear variation of $C_p = C_T + C_d$ with temperature T, can be expressed as $C_p = C_{p0} \exp(-E_A/kT)$, where C_{p0} is the preexponential term and E_A is the activation energy. The voltage dependent values of E_A were estimated from the slope of the resulting Arrhenius plots as about 0.017, 0.024 and 0.031 eV for 1.0, 0.9 and 0.7 V, respectively. The bias dependence of E_A suggest that the interface states which are proposed to be neutralized at higher voltages with significant carrier injection, and thus may be act also as recombination sites [17], which reduce the equivalent capacitance.

Fig. 3 also indicates that the value of equivalent parallel resistance decreases with increase in the temperature. This temperature dependent nature of R_p can be related with the temperature exponentially i. e., $R_p = R_{p0} \exp(E_{Ar/kT})$ where R_{p0} is the preexponential term and E_{Ar} is the activation energy of the process. The presence of (two for 0.9 V and 1.0 V and one for 0.7 V) linearly varying regions can be identified approximately below and above than 240 K in the figure. The value of E_{Ar} for a given dc bias voltage and region is estimated from the slope of from the related linear variation and as is shown in Fig. 3, E_{Ar} decreases with increase in the applied dc bias voltage for both regions. This behaviour can be interpreted as the increase of junction current as a result of junction barrier lowering [18]. It is quite difficult to identify the separate contributions of R_d or/and R_T to the equivalent parallel resistance, however for a typical *pn* based device in the dark, as the applied forward bias voltage increases the diode resistance R_d decreases. Since R_T is much greater than R_d, the parallel equivalent resistance is assumed to be close to R_d . The bulk resistance of the space charge region, R_d of a *pn* junction diode is defined as the ratio of a small change in applied voltage (dV) to the corresponding small change in current (dI) as

$$R_d = \frac{1}{dI/dV} = \frac{nkT}{qI},$$

where I is the diode current in the dark [19]. Thus the observed temperature dependent decrease of R_p can be attributed to the increase of junction current [15] and the leakage paths which can physically due to generation–recombination currents within the depletion region [17].

This observed dependence of equivalent parallel resistance on the temperature also implies that the conductance of the free charge carriers in this device follows the thermally activated current transport mechanism. More precisely, two different thermally activated routes can be identified approximately for $T > 240$ K and $T < 240$ K. It is also observed from Fig. 3 that as the value of dc voltage increases from 0.7 to 1.0 V, the value of R_p decreases while as the value of C_p increases. This opposite voltage dependent variation of R_p and C_p can also be attributed

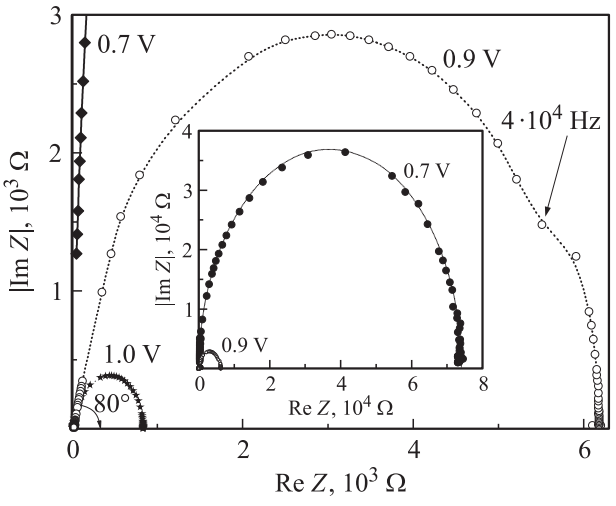

Figure 4. Room temperature impedance characteristics at $V_{dc} = 0.7$, 0.9 and 1.0 V.

to the increase of junction current as a result of junction barrier lowering [18].

The value of series resistance is found to be almost invariant around 15 Ω at 0.7 V and around 65 Ω at 0.9 V for the whole temperature region considered. But its value decreases gradually from 95 Ω to about 20 Ω when the temperature increases from 150 to 300 K at 1.0 V.

It has to be noted that a presence of some distorted region can be seen in Fig. 4 for impedance characteristics plotted for 0.9 V in the low frequency side ($f <\sim 10^4$ Hz) of the spectrum only for $T > 250$ K. The possible physical origin for such a deviation can be related to the presence of a second time constant (i. e., another *RC* sub-circuit) or electrically active defect states possibly located in the space charge region. However, the temperature dependent phase angle $\theta = \mathrm{tg}^{-1}(\mathrm{Im}\, Z/\mathrm{Re}\, Z)$ vs. $\lg f$ plots of the

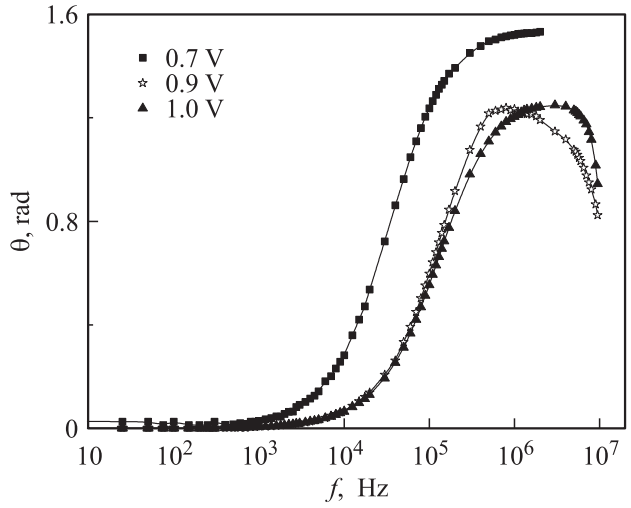

Figure 5. The phase angle $\theta = \mathrm{tg}^{-1}\left(\frac{\mathrm{Im}\, Z}{\mathrm{Re}\, Z}\right)$ vs. $\lg f$ plots at room temperature.

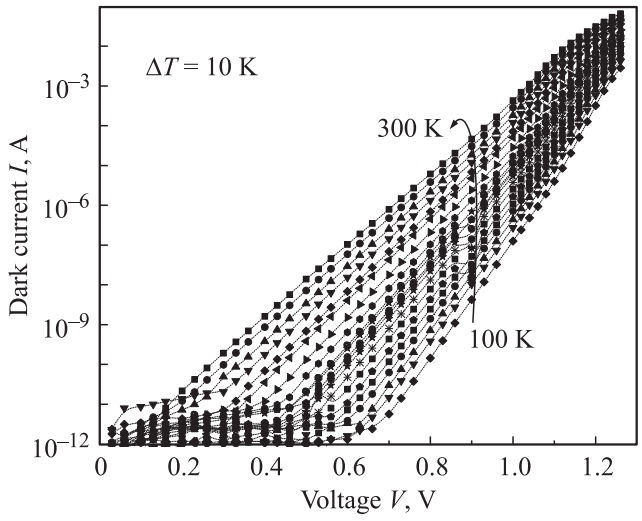

Figure 6. Forward $I-V$ characteristics at different temperatures. The dotted lines are present to guide the eye.

Temperature dependent values for diode ideality constant n and reverse saturation current I_0

$T(K)$	Region I		Region II	
	I_{01}, A	n_1	I_{02}, A	n_2
100	$1.79 \cdot 10^{-22}$	3.86	$1.00 \cdot 10^{-26}$	2.62
110	$1.26 \cdot 10^{-21}$	3.52	$4.30 \cdot 10^{-25}$	2.53
120	$4.60 \cdot 10^{-21}$	3.18	$2.50 \cdot 10^{-24}$	2.41
130	$4.50 \cdot 10^{-20}$	2.97	$2.00 \cdot 10^{-23}$	2.35
140	$8.79 \cdot 10^{-20}$	2.77	$1.50 \cdot 10^{-22}$	2.26
150	$3.50 \cdot 10^{-19}$	2.64	$1.98 \cdot 10^{-21}$	2.21
160	$1.18 \cdot 10^{-18}$	2.56	$3.26 \cdot 10^{-21}$	2.13
170	$1.73 \cdot 10^{-18}$	2.39	$1.57 \cdot 10^{-20}$	2.01
180	$8.70 \cdot 10^{-18}$	2.31	$5.67 \cdot 10^{-20}$	2.02
190	$1.14 \cdot 10^{-17}$	2.23	$3.29 \cdot 10^{-19}$	1.91
200	$6.29 \cdot 10^{-17}$	2.18	$1.57 \cdot 10^{-19}$	1.83
210	$2.17 \cdot 10^{-17}$	2.10	$9.77 \cdot 10^{-19}$	1.77
220	$4.30 \cdot 10^{-17}$	2.09	$1.35 \cdot 10^{-18}$	1.71
230	$1.29 \cdot 10^{-16}$	1.96	$8.53 \cdot 10^{-18}$	1.64
240	$3.90 \cdot 10^{-16}$	1.92	$3.77 \cdot 10^{-18}$	1.64
250	$1.93 \cdot 10^{-15}$	1.91	$1.39 \cdot 10^{-17}$	1.60
260	$7.39 \cdot 10^{-15}$	1.93	$1.38 \cdot 10^{-16}$	1.64
270	$2.53 \cdot 10^{-14}$	1.89	$8.10 \cdot 10^{-16}$	1.66
280	$5.99 \cdot 10^{-14}$	1.90	$7.90 \cdot 10^{-16}$	1.58
290	$1.89 \cdot 10^{-13}$	1.88	$8.30 \cdot 10^{-15}$	1.65
300	$4.29 \cdot 10^{-13}$	1.84		1.65

device at 0.7, 0.9 and 1.0 V have found to yield no other distinguishable peak like distribution for $f < 10^4$ Hz. The typical variation plotted at room temperature is illustrated in Fig. 5. Thus, the low frequency distortion seen in the complex impedance spectrum could possibly be related to electrically active defect states located at or near the junction interface.

In order to have a better understanding of the effect of temperature on the electronic properties of the space charge layer of the device and thus the interface states; current–voltage, I–V measurements are done. The forward $\lg I$ vs. V characteristic of the infrared emitting diode at various temperatures in the range of 100–300 K is given in Fig. 6. The forward current–voltage characteristics are expressed by the standard diode equation,

$$I = I_0 \exp\left(\frac{qV}{nkT}\right) \tag{3}$$

where n is the diode ideality factor, I_0 is the reverse saturation current and k is the Boltzmann's constant. The conduction mechanism was analysed by dividing the $\lg I$ vs. V characteristics into two distinct regions; I ($0.9 > V > 0.2$ V) and II ($V > 0.9$ V). The values of n and I_0 evaluated at different temperatures are tabulated in Table. In order to identify the dominant current transport mechanism through the device, the $\lg I_0$ was plotted as a function of T^{-1} as illustrated in Fig. 7. In both regions I and II, the plots are found to indicate visually good distinct linear variations with different slopes approximately

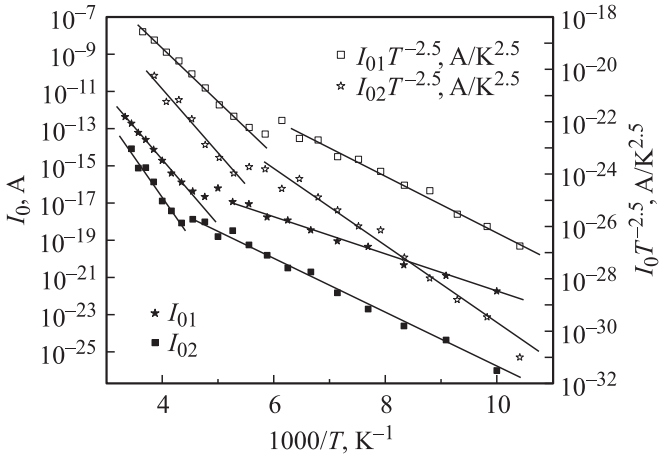

Figure 7. $\lg I_0$ and $\lg(I_0T^{-2.5})$ vs. Arhhenius plots at various temperatures.

below and above 230 K, indicating two different thermally activated routes for the current transport. As given in the Table, above 230 K the ideality factor n is almost constant at about 1.90 and 1.64 in region I and II, respectively. However below 230 K, n values increases slightly with decreasing temperature. All of these results are indicative of a pure thermally activated phenomenon above 230 K for which I_0 is expressed as

$$I_0 = I_{00} \exp\left(\frac{-\Delta E}{kT}\right) \tag{4}$$

where ΔE the activation energy and I_{00} a prefactor which depends on the transport mechanism. If, junction recombination trough the interface plane dominates the current transport the value of n should be in between 1 to 2 depending on the impurity concentrations of the n and p layers, and the product ΔEn should be around the built-in voltage V_{bi} of the junction. The room temperature value of V_{bi} is estimated as about 3.88 V by high frequency (1 MHz) capacitance–voltage measurement. From the slope of $\lg I_0$ vs. $1000/T$ plots for temperatures almost above 230 K, the activation energies were estimated to be about 0.694 and 0.855 eV for region I and II, respectively. The corresponding built-in voltage values calculated from ΔEn are found to be 1.318 and 1.402 eV for regions I and II, respectively, which are quite smaller than the expected value of V_{bi}. Thus, we can propose that the interface state recombination mechanism is not the dominating route.

If depletion region recombination dominates, the distribution of defect states in the space charge region provides n values varying in between 11 to well above to 2 [20] and the slope of the $\lg(I_0T^{-2.5})$ vs. $1000/T$ plot must yield an activation energy approximately equal to the half of the band gap of the depletion layer. If the active layer of the device is simply GaAs, the value of the energy gap at around space charge layer is expected to be about 1.42 eV. The values for the activation energy are found as around 0.642 and 0.762 eV for region I and II, respectively from the slope of the $\lg(I_0T^{-2/5})$ vs. $1000/T$ plot (see Fig. 7). These activation energy values are not equal to the half of the GaAs band gap of 1.42 eV but actually we do not know the definite energy band diagram and the doping profiles of different layers in the device. Thus it is difficult precisely declare the validity of the depletion recombination mechanism in the device. Nevertheless, relatively low $I_0(T)$ values, high diode performance i. e., high rectification ratio ($\sim 10^5$ at 0.5 V) and the relatively low values of the diode ideality factor of the device may suggest that recombination through defect states in the depletion region could possibly be the dominating route for the current transport.

Below 230 K, the values of the diode ideality factor are not constant, $n(T) > 1$ and the slopes of the $\lg I = f(V)$ plots vary very slowly with temperature for both region I and region II. This behaviour indicates that the proposed thermally activated path could be enhanced by tunneling through defect states at or close to the junction interface [20,21].

4. Conclusion

The ac and the dc responses of a commercially available GaAs based infrared emitting diode have been studied with impedance spectroscopy and current–voltage measurements respectively, in the dark. The impedance spectroscopy data measured at different temperatures (150–300 K) have indicated that the device behaves as a capacitor for dc bias voltages below than 0.7 V. Above 0.7 V, the spectra obtained at each temperature are simulated fairly well by an equivalent circuit model composed by a single R_pC_p network with a series resistor. At 0.9 V and 1.0 V, the equivalent capacitance of the device is found to be due to transition capacitance approximately above 270 K beyond this and for 0.7 V, the diffusion capacitance dominates. This is attributed to be due to the presence of interfacial trapping states responding to the applied ac signal. Since the applied forward dc bias voltage is high enough, the parallel equivalent resistance can be safely assumed to be close to the bulk resistance of the space charge region. The temperature dependent nature of the equivalent parallel resistance is shown to be related with the temperature exponentially and the presence of two different thermally activated regions is distinguished.

The current transport mechanism in the dark proposed to be dominated by depletion recombination approximately above 230 K. However below about 230 K, the effect of tunneling to the proposed thermally activated path was suggested.

References

[1] Vishay Telefunken, *Data sheets of CQY37N Infrared Emitting Diode*. http://www.vishay.com/docs/81002/81002.pdf

[2] E. Peiner, K. Fricke, D. Fehly, A. Schlachetzki, P. Hauptmann. Sensors and Actuators A, **68**, 249 (1998).
[3] N.C. Das, J. Bradshaw, F. Towner, R. Leavitt, Solid-State Elec. **52**, 1821 (2008).
[4] P. Szûcs, V. Pintoa, B.V. Safronova. J. of Neuroscience Met. **177**, 369 (2009).
[5] J.R. Macdonald. *Impedance Spectroscopy* (John Wiley and Sons, New York, 1987).
[6] E. Barsoukov, J.R. Macdonald. *Impedance Spectroscopy: Theory, Experiment and Application* (John Wiley and Sons Inc, Haboken, New Jersey, 2005).
[7] H. Bayhan, A.S. Kavasoğlu. Sol. Energy **80**, 1160 (2006).
[8] Y.Y. Proskuryakov, K. Durose, B.M. Taele. J. of App. Phys. **102**, 024 504 (2007).
[9] L. Wu, Y. Ogawa, A. Tagawa. J. Food Eng. **87**, 274 (2008).
[10] Y. Li, J. Gao , G. Yu, Y. Cao, A.J. Heeger. Chem. Phys. Lett. **287**, 83 (1998).
[11] L.S.C. Pingree B.J. Scott, M.T. Russell, T.J. Marks, M.C. Hersam. Appl. Phys. Lett., **86**, 073 509 (2005).
[12] T. Okachi, T. Nagase, T. Kobayashi, H. Naito. Appl. Phys. Lett., **94**, 043 301 (2009).
[13] H.S. Raushenbach. **Solar Array Design Hand Book** (Van Nostrand Reinhold, New York, 1980).
[14] M.S. Suresh. Sol. Energy Mat. and Solar Cells, **43**, 21 (1996).
[15] R.A. Kumar, M.S. Suresh, J. Nagaraju. Sol. Energy Mat. and Solar Cells, **85**, 397 (2005).
[16] E. Schibli, A.G. Milness. Solid State Electron., **11**, 323 (1968).
[17] W.A. Strifler, C.W.Bates, J. Appl. Phys., **71**, 4358 (1992).
[18] R.A. Kumar, M.S. Suresh, J. Nagaraju. Sol. Energy Mat. and Solar Cells **77**, 145 (2003).
[19] Halkias Millman. *Integrated electronics* (McGraw-Hill, New York, 1972).
[20] A.L. Fahrenbruch, R.H. Bube. *Fundamentals of Solar Cells* (Academic Press, 1983).
[21] V. Nadenau, U. Rau, A. Jasenek, H.W. Schock. J. Appl. Phys., **87**, 584 (2000).

Редактор Т.А. Полянская